Dynamics of water probed with vibrational echo correlation spectroscopy

John B. Asbury, Tobias Steinel, and Kyungwon Kwak
Department of Chemistry, Stanford University, Stanford, California 94305

S. A. Corcelli, C. P. Lawrence, and J. L. Skinner
Department of Chemistry, University of Wisconsin, Madison, Wisconsin 53706

M. D. Fayer
Department of Chemistry, Stanford University, Stanford, California 94305

(Received 17 August 2004; accepted 22 September 2004)

Vibrational echo correlation spectroscopy experiments on the OD stretch of dilute HOD in H_2O are used to probe the structural dynamics of water. A method is demonstrated for combining correlation spectra taken with different infrared pulse bandwidths (pulse durations), making it possible to use data collected from many experiments in which the laser pulse properties are not identical. Accurate measurements of the OD stretch anharmonicity (162 cm^{-1}) are presented and used in the data analysis. In addition, the recent accurate determination of the OD vibrational lifetime (1.45 ps) and the time scale for the production of vibrational relaxation induced broken hydrogen bond ''photoproducts'' ($\sim$2 ps) aid in the data analysis. The data are analyzed using time dependent diagrammatic perturbation theory to obtain the frequency time correlation function (FTCF). The results are an improved FTCF compared to that obtained previously with vibrational echo correlation spectroscopy. The experimental data and the experimentally determined FTCF are compared to calculations that employ a polarizable water model (SPC-FQ) to calculate the FTCF. The SPC-FQ derived FTCF is much closer to the experimental results than previously tested nonpolarizable water models which are also presented for comparison. [DOI: 10.1063/1.1818107]

I. INTRODUCTION

The dynamics and structure of water continue to be a problem of both fundamental interest and practical significance. Water is important as a solvent in a vast number of chemical and biological settings. To a great extent, the unique properties of water derive from its ability to form complex hydrogen bond networks.[1] Water can form up to four hydrogen bonds, but the number and strength of the hydrogen bonds continually fluctuate.[2–5] Therefore, understanding the dynamics of the hydrogen bond networks is central to understanding the nature of water. Characterization of the full dynamics of the hydrogen bond networks is essential to test water models which find application in simulations of protein folding,[6,7] ion hydration,[8] and polymerization reactions.[9]

While there have been a wide variety of experimental methods directed at understanding water, ultrafast infrared experiments that examine the water hydroxyl stretching mode are particularly well suited for the study of the hydrogen bond network dynamics. The frequency of the hydroxyl stretch is sensitive to the strength of the hydrogen bonds and the number of hydrogen bonds.[2,3,10–13] The distribution in the strengths and number of hydrogen bonds gives rise to the very broad hydroxyl stretch absorption line observed in IR spectra of water.[2,3] However, the different strengths and numbers of hydrogen bonds do not give rise to spectroscopically resolvable features in the water spectrum. For that reason, a number of ultrafast infrared experimental methods have been applied to extract information about hydrogen bond dynamics from under the inhomogeneously broadened hydroxyl stretch absorption band.[5,14–35]

The development of the ultrafast infrared vibrational echo technique,[36–39] and the application of vibrational echo experiments to the study of water,[5,15–19,40] provide a direct method for accessing hydrogen bond dynamics through the hydroxyl stretch frequency evolution. Vibrational echo correlation spectroscopy experiments with full phase information applied to water[5,19] can provide more detailed examination of water dynamics than two pulse vibrational echoes[18] or vibrational echo peak shift measurements.[15–17] The multidimensional stimulated vibrational echo correlation spectroscopy technique measures the population and vibrational dephasing dynamics in two frequency dimensions ω_τ and ω_m.[5,41–46] (In NMR, ω_τ and ω_m are usually called ω_1 and ω_3, respectively.[47]) The ω_m axis is similar to the frequency axis in frequency resolved pump-probe spectroscopy. The ω_τ axis does not have an analog in the pump-probe experiment; it provides an additional dimension of information that is contained only in the correlation spectrum. The time evolution of the shapes of the bands in the correlation spectra provides information on the dynamics of the system produced by structural evolution of the hydrogen bond network.

In the experiments, ultrashort mid-IR pulses, ($\sim$50 fs or $<$4 cycles of light), were employed, making it possible to perform experiments on the entire broad hydroxyl stretching band despite its $>$400 cm^{-1} width. Employing pulses that are transform limited and controlling path lengths with accuracy of a small fraction of a wavelength of light, along with

proper analysis, data are obtained with correct phase relationships across the entire spectrum. The proper phase relationships permit accurate separation of the absorptive and dispersive contributions to the spectra.[5,42,44,48] As a result, the two-dimensional (2D) IR correlation spectra are obtained in a manner akin to 2D NMR spectroscopy.[47]

The OD hydroxyl stretch of dilute HOD in H_2O was investigated previously with vibrational echo correlation spectroscopy experiments on water.[5] The results were compared to theoretically calculated results[3,5,49] obtained from two water simulation models TIP4P (Ref. 50) and SPC/E.[51] Below we present supplementary vibrational echo correlation spectroscopy experiments on water and compare them to additional simulations.

The vibrational echo correlation spectra are measured as a function of the time delay T_w between the second and third pulses in the stimulated vibrational echo pulse sequence. The resulting T_w dependent data are fit by varying the frequency time correlation function (FTCF), which is input into a time dependent diagrammatic perturbation theory calculation of the data.[41,52] In addition, the FTCF obtained from the experiments is compared to calculations based on the SPC-FQ (Ref. 53) water model. A quantum oscillator is embedded in the classical molecular dynamics simulation to calculate the FTCF.[3,5,49,54] The resulting FTCF is then input into a diagrammatic perturbation theory calculation to obtain simulated data in the same form as the experimental data. The previous calculations using the TIP4P and SPC/E models showed relatively poor agreement with the experiments, particularly at long time. In contrast, calculations of the FTCF using the SPC-FQ model[54] are in much better agreement with the data. The better agreement may occur because the polarizable term in the SPC-FQ model introduced collective effects into the molecular dynamics simulation. These collective effects are absent in the TIP4P and SPC/E models because they are do not contain the polarizable term. The experiments have improved accuracy and data analysis procedures. In addition, complementary experiments have been performed to obtain data that are necessary for the analysis of the vibrational echo experiments. Using spectrally resolved ultrafast IR pump-probe experiments, the vibrational anharmonicity of the OD stretch of HOD in water is accurately determined (162 cm^{-1}). The anharmonicity is a necessary input parameter in the diagrammatic perturbation theory calculations used to extract the FTCF from the data and to compare the data to the simulations. Furthermore, an accurate value of the OD stretch lifetime (1.45 ps) (Ref. 55) was employed. The determination of the lifetime took into account the generation of ''photoproducts'' (broken hydrogen bonds) that are formed following vibrational relaxation.[55] The production of photoproducts changes the hydroxyl stretch spectrum and influences the determination of the vibrational spectral diffusion. Detailed analysis of the growth of the photoproduct spectrum demonstrates that the photoproducts do not significantly impact the vibrational echo correlation spectra because of the relatively long lifetime of the OD stretch in H_2O. This is one of the reasons that OD in H_2O is studied rather than OH in D_2O.[15–18] OH in D_2O has a substantially shorter lifetime ($\sim$0.7 ps).[56,57] The generation of photoproducts limits the time over which OH in D_2O results can be analyzed in a straightforward manner, a factor that has not been taken into account in previous reports.[17,18]

II. EXPERIMENTAL PROCEDURES

The ultrashort IR pulses employed in the experiments are generated using a Ti:sapphire regeneratively amplified laser/OPA system. The output of the modified Spectra Physics regen is 26 fs transform limited 2/3 mJ pulses at 1 kHz rep rate. These are used to pump an optical parametric amplifier (BBO) employing difference frequency generation ($AgGaS_2$). The output of the OPA is compressed to produce $\sim$50 fs transform limited IR pulses as measured by collinear autocorrelation. For the experiments, the compression was readjusted to give transform limited pulses in the sample as measured by a sample that gave a purely nonresonant signal. The pulses were always transform limited in the sample during the course of an experiment, that is, over the full range of T_ws. However, over the several months during which data were collected, there was some variation in the bandwidth (pulse duration) of the pulse. A change in bandwidth has a substantial influence on the experimental correlation spectra, as discussed below. As detailed in the Appendix, a method was developed to combine data sets taken with different pulse bandwidths. Therefore, it is possible to average together data sets taken under appropriate but not identical conditions.

The IR beam is split into five beams. Three of the beams are the excitation beams for the stimulated vibrational echo. A fourth beam is the local oscillator (LO) used to heterodyne detect the vibrational echo signal. One of the excitation beams is also used for pump-probe experiments, with the fifth beam as the probe beam in the pump-probe experiments. All of the beams that pass through the sample are optically identical and are compensated for group velocity dispersion simultaneously. The vibrational echo signal combined with the LO is passed through a monochromator and detected by a 32 element MCT array. At each monochromator setting, the array detects 32 individual wavelengths.

The sample, 5% HOD in H_2O, was held in a sample cell of CaF_2 flats with a spacing of 6 μm. The peak absorbance of the samples was 0.2. Such a low absorbance is necessary to prevent serious distortions of the pulses as they propagate through the sample. The OD stretch of HOD is used as a probe of water for three reasons. The relatively dilute OD stretch reduces the rate of vibrational excitation transport to the point where transport has a negligible influence on the dynamics.[58] Excitation transport would be a source of spectral diffusion that is not related to structural dynamics of water. Furthermore, it is very difficult to make a pure water sample that is thin enough to have the necessary low optical density for the experiments, and such a thin sample is subject to heating artifacts. Finally, as discussed below and mentioned in the Introduction, the vibrational lifetime of the OD stretch of HOD in H_2O and the time for the onset of the photoproduct spectrum caused by hydrogen bond breaking determine the longest time for which data can be taken and

unambiguously interpreted. The OD stretch of HOD in H_2O lifetime is significantly longer than the OH stretch lifetime in D_2O.

The phase-resolved, heterodyne detected, stimulated vibrational echo was measured as a function of one frequency variable ω_m and two time variables τ and T_w that are defined as the time between the first and second sample-radiation field interactions and the second and third sample-radiation field interactions, respectively. The measured signal is the absolute value squared of the sum of the vibrational echo signal electric field S and the local oscillator electric field L

$$|L+S|^2 = L^2 + 2LS + S^2. \tag{1}$$

The L^2 term is time independent and the S^2 is very small; hence neither contributes to the time dependence of the signal. The $2LS$ term is the heterodyne amplified signal. The monochromator performs an experimental Fourier transform on the radiation. Through data processing that involves chopping to measure L^2 and normalization, the spectrum yields the ω_m frequency axis. As the τ variable is scanned in 2 fs steps, the phase of the vibrational echo signal electric field is scanned relative to the fixed local oscillator electric field, resulting in an interferogram measured as a function of the τ variable. The interferogram contains the amplitude, sign, frequency, and phase of the vibrational echo signal electric field as it varies with τ. By numerical Fourier transformation, this interferogram is converted into the frequency variable ω_τ, providing the ω_τ axis.

The interferogram measured as a function of τ contains both the absorptive and dispersive components of the vibrational echo signal. However, two sets of quantum pathways can be measured independently by appropriate time ordering of the pulses in the experiment.[43,44,46] With pulses 1 and 2 at the time origin, pathway 1 or 2 is obtained by scanning pulse 1 or 2 to negative time, respectively. Adding the Fourier transforms of the interferograms from the two pathways, the dispersive component cancels leaving only the absorptive component. The 2D vibrational echo correlation spectra are constructed by plotting the amplitude of the absorptive component as a function of both ω_m and ω_τ.

Lack of perfect knowledge of the timing of the pulses and consideration of chirp on the vibrational echo pulse requires a ''phasing'' procedure to be used.[5,40] The projection slice theorem[47] with an auxiliary condition is employed to generate the absorptive 2D correlation spectrum. The projection of the absorptive 2D correlation spectrum onto the ω_m axis is equivalent to the IR pump-probe spectrum recorded at the same T_w, as long as all the contributions to the stimulated vibrational echo are absorptive. Consequently, comparison of the projected 2D stimulated vibrational echo spectrum to the pump-probe spectrum permits the correct isolation of the absorptive vibrational echo correlation spectrum from the 2D spectrum obtained from the addition of the two quantum pathways.

It is possible to come relatively close to the correct correlation spectrum prior to the phasing procedure because the very short pulses permit their time origins to be known within a few femtoseconds. However, the correlation spectrum is very sensitive to small errors in the time origin, even on the order of 1 fs, and to chirp. Therefore, a well defined phasing procedure based on various potential errors was developed.[45,59] The frequency dependent phasing factor used to correct the 2D spectra has the form

$$\begin{aligned} S_C(\omega_m,\omega_\tau) &= S_1(\omega_m,\omega_\tau)\Phi_1(\omega_m,\omega_\tau) \\ &\quad + S_2(\omega_m,\omega_\tau)\Phi_2(\omega_m,\omega_\tau), \\ \Phi_1(\omega_m,\omega_\tau) &= \exp[\,i(\omega_m\Delta\tau_{\mathrm{LO},E} + \omega_\tau\Delta\tau_{1,2} + \omega_m\omega_\tau C \\ &\quad + \omega_m^2 Q)\,], \\ \Phi_2(\omega_m,\omega_\tau) &= \exp[\,i(\omega_m\Delta\tau_{\mathrm{LO},E} - \omega_\tau\Delta\tau_{1,2} + \omega_m\omega_\tau C \\ &\quad + \omega_m^2 Q)\,]. \end{aligned} \tag{2}$$

S_C is the correlation spectrum. S_1 and S_2 are the spectra recorded for pathways 1 and 2, respectively. $\Delta\tau_{\mathrm{LO},E}$ accounts for the lack of perfect knowledge of the time separation of the LO pulse and the vibrational echo pulse; $\Delta\tau_{1,2}$ accounts for the lack of perfect knowledge of the time origins of excitation pulses 1 and 2; C accounts for linear chirp caused by the echo propagating through the sample; and Q accounts for the linear chirp caused by propagation of the vibrational echo through the back window of the sample cell. $\Delta\tau_{1,2}$ comes in with opposite sign for pathways 1 and 2.

An additional procedure was developed and employed to produce the very high quality correlation spectra shown below.[5,40] The projection slice theorem reduces a two-dimensional entity to a one-dimensional entity. However, in order to unambiguously assign a correct correlation spectrum it is preferable to use information from both dimensions. Therefore, in the phasing procedure an additional constraint is applied for the ω_τ dimension. We can use information from the absolute value correlation spectrum, which is the sum of the absolute value spectra of pathway 1 (rephasing) and pathway 2 (nonrephasing) discussed above. The absolute value spectrum is independent of the phase factor and peaks at the same frequency along ω_τ as the purely absorptive spectrum. Consequently, the difference in peak positions of a trial phased absorptive spectrum and the absolute value spectrum for each ω_m gives an additional criterion on the quality of the correlation spectrum. The correct correlation spectrum is the one that provides the best fit to the pump-probe spectrum and minimizes the difference in peak positions of the absorptive and absolute value spectra. This procedure holds for symmetric line shapes and hence can be applied to the data discussed here, where the dynamical lines can be well fit to a Gaussian line shape and the deviations are symmetric.

Finally, to test the procedures described above and to make final very small corrections, a method call PEARL for ''phasing employing absorptive resonant loci'' was used. This procedure will be discussed in detail subsequently.[60] PEARL is the multidimensional, multipeak absorptive equivalent of a Cole-Cole procedure used in dielectric relaxation experiments.[60] Following phasing, the errors in the time origins are $<100\times10^{-16}$ s and the time shift across the entire spectrum due to chirp $\omega_m C$ is $<100\times10^{-16}$ s.

III. RESULTS AND DISCUSSION

The hydroxyl stretch frequency provides a sensitive probe of the hydrogen bond dynamics of water through its correlation with the strength and number of hydrogen bonds associated with a water molecule.[2,3,10–13] Ultrafast time-resolved nonlinear vibrational spectroscopy probes the hydroxyl stretch directly, and so provides access to the hydrogen bond dynamics. Vibrational echo spectroscopy[36–39] and, in particular, multidimensional vibrational echo correlation spectroscopy[5,19,40,61] provides superior time resolution and sensitivity to the dynamics of water compared to IR pump-probe techniques.[20–27,33–35] Multidimensional vibrational echo correlation spectroscopy provides experimental observables that permit the parametrization or selection of the most accurate water models.[5,54]

Significant disparities exist between recent measurements of water dynamics made by several groups using different vibrational echo techniques.[5,17–19] The water dynamics are described by the FTCF that each group reported. The FTCF is defined as

$$C(t) = \langle \delta\omega(t)\,\delta\omega(0)\rangle, \tag{3}$$

where $\delta\omega$ is the change in the hydroxyl stretch frequency from its initial value, and the bracket is an ensemble average. The FTCF describes the loss of correlation of the frequency of an ensemble of OD stretches as time progresses. Yeremenko, Pshenichnikov, and Wiersma heterodyne detected a 2-pulse vibrational echo of the OH stretch of HOD in D_2O[18] and reported a biexponential decaying FTCF with 130 and 900 fs time constants having ~60% and ~40% amplitudes, respectively. Fecko *et al.* also studied the OH stretch of HOD in D_2O using 3-pulse vibrational echo peak shift measurements.[17] They reported a FTCF that decayed in ~200 fs (~85% amplitude) with a large oscillation followed by a 1.2 ps exponential decay (~15% amplitude). Both aforementioned experiments utilized frequency integrated techniques which did not discriminate between the 0-1 and 1-2 transitions that are emitted by the hydroxyl stretch and so included both ground and excited state dynamics in their measurements. Most recently, the OD stretch of HOD in H_2O was studied using vibrational echo correlation spectroscopy. The experiments yielded a FTCF described by a triexponential function having 32 fs, 400 fs, and 1.8 ps time constants with corresponding 43%, 16%, and 41% amplitudes.[5,19] These experiments selectively measured the dynamics of the 0-1 transition because the vibrational echo correlation spectroscopy technique spectrally resolves the vibrational echo and facilitates complete discrimination between ground and excited state contributions. A review of other reports of the FTCF of water has been provided recently.[5]

The differences in the dynamics of water reported in these three experimental investigations[5,17–19] suggest that the experimental execution and the experimental method can influence the results. To improve the experimental accuracy of the vibrational echo correlation spectroscopy measurements on water, we have performed the type of experiments reported above[5,19] with improved technique five times over the course of many months and under many different laser conditions. Additionally, we have performed complementary experiments to obtain properties of the hydroxyl stretch that are more accurate than those available in the literature. These auxiliary experiments are necessary for accurate analysis of the vibrational echo experiments and accurate determination of the FTCF using molecular dynamics simulations of three water models.

This report is broken into two main sections: (A) measurement of water dynamics and (B) comparison of experimental and theoretical dynamics predicted from three models of water. Within Sec. III A, we describe our measurement of the vibrational anharmonicity and the vibrational lifetime of the hydroxyl stretch using spectrally resolved infrared pump-probe spectroscopy.[55] We then present the results from five sets of vibrational echo correlation spectra and discuss data analysis procedures that enable us to combine multiple data sets to reduce the error bars in the measurement. Section III B compares the experimental data with predictions from three water models and discusses the differences between the models that affect their predicted dynamics.

A. Accurate measurement of water dynamics

1. OD stretch anharmonicity

The goal of studying the vibrational dynamics of water is to access the ground state equilibration dynamics, which are displayed in the 0-1 transition. The 1-2 transition reports the dynamics of the excited state, which is not the principle objective of the study. The 1-2 transition of the OD stretch vibration of HOD in liquid water significantly overlaps the 0-1 transition. The contribution of the 1-2 transition in the experimental data can be accounted for as long as the anharmonicity (shift in frequency between the 0-1 and 1-2 transitions) is known accurately. The ground state dynamics of water can be measured from the 0-1 transition once the contribution from the 1-2 transition is known. The dynamics can be examined at wavelengths that do not have interference from the 1-2 transition in the frequency resolved correlation spectroscopy experiments. In addition, the contribution of the 1-2 transition can be calculated using diagrammatic perturbation theory.[5,41,52,62,63] The calculations describe the 0-1 and 1-2 transitions and require the anharmonicity as input. By comparing the experimental data with the calculated results, the ground state dynamics can be obtained without any contamination from the excited state.[5,19]

The anharmonicity of the OD stretch vibration of HOD in liquid water has been reported several times with values ranging from 127 (Ref. 64) to ~200 cm^{-1}.[33] The uncertainty in the values from the literature is far greater than can be tolerated in the analysis of the experiments. Consequently, we determined the anharmonicity of the OD stretch of HOD in H_2O using frequency resolved pump-probe spectroscopy.

The pump-probe spectra at delay times T_w shorter than the vibrational lifetime are composed of the bleach of the 0-1 transition and the excited state absorption of the 1-2 transition. A representative difference spectrum collected at $T_w = 200$ fs is displayed in Fig. 1. The bleach of the ground state is a positive signal centered at 2510 cm^{-1}, while the negative excited state absorption signal is centered around 2350 cm^{-1}. To extract a precise anharmonicity constant, we fit the pump-

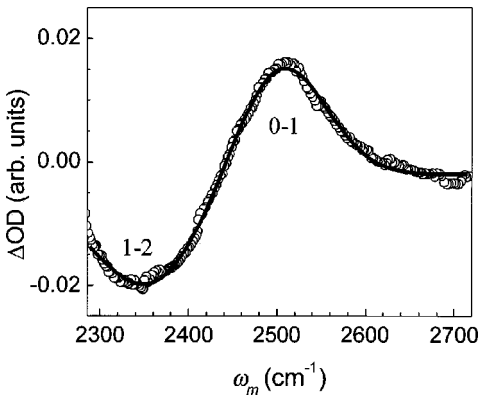

FIG. 1. Transient absorption spectrum of the OD hydroxyl stretch of HOD in water collected at pump-probe delay $T_w = 0.2$ ps. The 0-1 transition is positive going at ~2510 cm^{-1} and the 1-2 transition is negative going at ~2350 cm^{-1}. The solid line through the data is a fit comprised of two Gaussians, one for the 0-1 and another for the 1-2 transition that yields the anharmonicity 162 cm^{-1}.

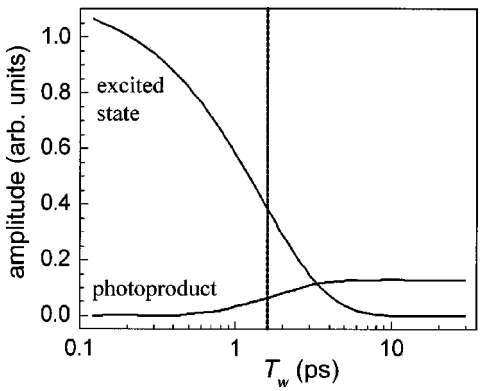

FIG. 2. Time dependent contributions to the signal of the initially excited (upper curve) and photoproduct (lower curve) populations of water species measured from transient absorption experiments. The photoproduct forms following vibrational relaxation of the hydroxyl stretch, which breaks hydrogen bonds.

probe spectrum to a sum of two Gaussian line shapes, one corresponding to the ground state and another to the excited state. The fit is displayed as the solid line through the data in Fig. 1. We obtained a more constrained fit by fixing the center of the ground state peak to be the same as the peak of the OD-hydroxyl stretch absorption in the Fourier transform infrared absorption spectrum (2510 cm^{-1}) (Ref. 5) while leaving the center of the 1-2 transition and the widths of the Gaussians as fitting parameters. We performed the fit described above on hundreds of distinct pump-probe spectra at delay times ranging from 0.12 to 1.0 ps. The difference between the peak positions of the 0-1 and 1-2 transitions that were determined from the fits provides the anharmonicity constant, which we determined to be 162 ± 4 cm^{-1}.

2. OD stretch lifetime and photoproduct formation

The vibrational lifetime of the hydroxyl stretch determines the time duration over which the equilibrium dynamics of water can be unambiguously measured. Beyond this time window, photoproducts that result from hydrogen bond breaking contribute to the signal.[55] If the dynamics of water are measured on the time scale of and beyond the vibrational lifetime, the measured dynamics do not solely reflect the equilibrium fluctuations of water. The photoproducts of hydrogen bond breaking that form following vibrational relaxation contaminate the signal.[55] To determine the time window during which the ground state fluctuations of water may be interrogated and to access the contribution to the signal from the production of photoproducts as a function of time, the vibrational lifetime was determined using broadband transient absorption experiments to monitor the hydroxyl stretch population dynamics.[55] The ultrashort mid-IR pulses (~50 fs or <4 cycles of light) uniformly excited the 0-1 transition of the OD hydroxyl stretch of HOD in water, which completely eliminated the influence of spectral diffusion from the dynamics. Such precautions have not always been taken into account previously.[20–27,33–35] The ultrafast transient absorption experiments have been described in detail elsewhere.[55] The necessary details are recounted here to establish the T_w delays, for which the generation of photoproducts can influence the measurements of the dynamics of water. The magnitude of the influence of the photoproducts on the vibrational echo results are determined quantitatively below.

The transient absorption spectra were taken in a magic angle configuration to eliminate orientational dynamics.[55] The transient spectra were decomposed into reactant and photoproduct contributions using singular value decomposition.[55,65] Separation of the vibrational relaxation dynamics from the hydrogen bond breaking and formation processes revealed an exponential vibrational lifetime of $\tau_{vib} = 1.42 \pm 0.05$ ps across the entire hydroxyl stretch band including 0-1 and 1-2 transitions. As a consistency check we analyzed the data by fitting the transient absorption decay at the red side of the 1-2 transition, where the decay is not perturbed by the photoproduct dynamics. The results were virtually the same and the vibrational lifetime was found to be frequency independent with a time constant $\tau_{vib} = 1.45 \pm 0.05$ ps. This value for the lifetime[55] is slightly shorter and much more accurate than previous measurements.[33,35]

From the measurement of the population dynamics, which is briefly discussed here, it was demonstrated that excitation of the hydroxyl stretch and subsequent vibrational relaxation breaks hydrogen bonds and produces spectrally distinct photoproducts.[55] Figure 2 displays the spectrally resolved dynamics of the initially excited and the photoproduct populations at 2500 cm^{-1} (note the time scale is logarithmic). The excited state contribution to the signal (upper curve) decays exponentially (1.45 ps), while the photoproduct (lower curve) grows in nonexponentially as a result of the vibrational relaxation rate and the hydrogen bond breaking rate (810 fs).[55] The dashed line indicates the maximum T_w delay at which a correlation spectrum is reported in this work. It is clear that the measured dynamics will not be substantially affected by the photoproducts for $T_w < 1$ ps, while at times larger than 5 ps the photoproduct prevails. At intermediate times both components contribute to the transient absorption signal and neither of them can be neglected. From the analysis, the photoproduct contributes to the tran-

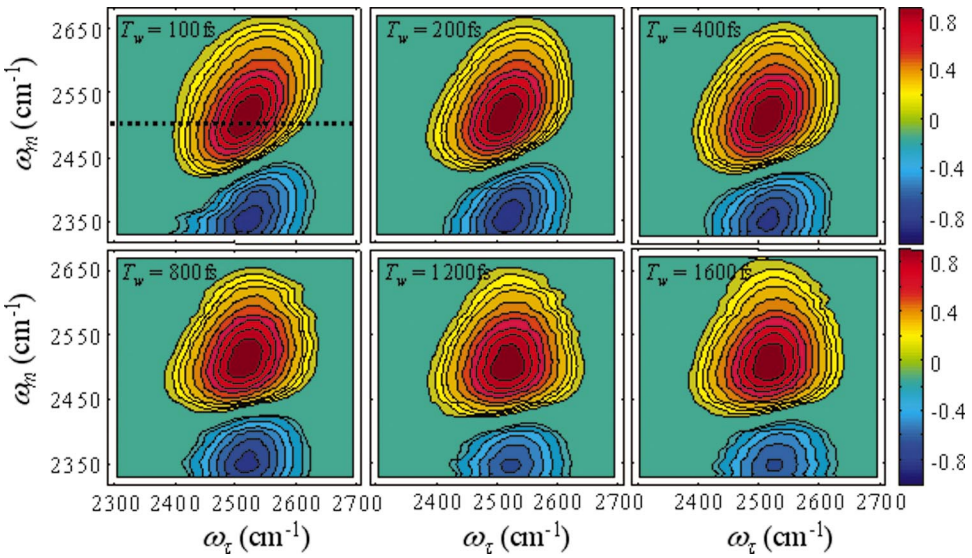

FIG. 3. (Color) The experimental vibrational echo correlation spectra of the OD stretch of HOD in H_2O. The data have been normalized to the maximum positive value. Each contour represents a 10% change. The positive going peak arises from the 0-1 transition. The negative going peak arises from the 1-2 transition. The 0-1 and 1-2 peaks are elongated along the diagonal, indicating inhomogeneity persists in the hydroxyl stretch frequency distribution. Spectral diffusion broadens the widths of the peaks as T_w increases. The dashed line represents a cut at $\omega_m = 2500\ \mathrm{cm}^{-1}$.

sient absorption signal ~3%, 8%, and 15% of the total at T_w delays of 800, 1200, and 1600 fs, respectively.

The influence of the photoproduct on the vibrational echo correlation spectra is discussed in detail below. From the analysis, the photoproduct signal contributes only ~0.5 cm^{-1} to the measured dynamic line width at the longer T_w delays, (800–1600 fs) which is negligible given that the error bars in the measurement are $\pm 2.5\ \mathrm{cm}^{-1}$ (see below). Consequently, it is unnecessary to correct the measured dynamic linewidths for the photoproduct contribution. As has been discussed in detail elsewhere,[55] the growth of the photoproducts does have a significant influence on the determination of the vibrational lifetime and the orientational relaxation.

3. Vibrational echo correlation spectra

Since the first report of vibrational echo correlation spectroscopy experiments investigating the dynamics of water,[5] we have refined the data collection and analysis methods to enhance the accuracy of the measurements of water dynamics. The results of Secs. III A 1 and 2 are used below in the analysis presented in this section. Five distinct sets of time dependent correlation spectra were collected to improve the accuracy. The data sets were collected over the span of several months. Each data set comprised an independent collection of correlation spectra measured for six T_w points at 100, 200, 400, 800, 1200, and 1600 fs. A typical set of correlation spectra from a single experiment is displayed in Fig. 3. The correlation spectra are two-dimensional frequency maps of the frequency fluctuations of the OD stretch. The ω_τ axis (horizontal axis) displays the frequency of the interaction of the sample with the first laser pulse, which occurs at the 0-1 transition frequency in the region around 2500 cm^{-1}. All the features in the correlation spectra appear centered at the 0-1 transition frequency along the ω_τ axis. The ω_m axis displays the frequency at which the vibrational echo is emitted from the sample. Vibrational echo correlation spectroscopy accesses the ground (0), first (1), and second (2) vibrational states. Consequently, two peaks are observed along the ω_m axis corresponding to the 0-1 and the 1-2 transition frequencies. The positive going 0-1 peak appears on the diagonal (represented by the line $\omega_m = \omega_\tau$) because the vibrational echo is emitted with the same frequency as the first interaction with the radiation field (first pulse). The negative going peak corresponds to the vibrational echo that was emitted on the 1-2 transition. The peak appears redshifted along the ω_m axis by the anharmonicity $\Delta_{\mathrm{an}} = 162\ \mathrm{cm}^{-1}$ (Sec. III A 1) because the vibrational echo was emitted from the 1-2 transition, but the first interaction was with the 0-1 transition. Similar to IR transient absorption spectroscopy, the 0-1 peak is positive and the 1-2 peak is negative because they result from a decrease in the ground state population and an increase in the excited state population, respectively. The phase resolution afforded by heterodyne detected vibrational echo correlation spectroscopy displays the sign parity between the 0-1 and 1-2 transitions. The sign parity combined with the measurement of purely absorptive line shapes facilitates the complete removal of the excited state contribution from the ground state dynamics, unlike previous investigations of water dynamics.[17,18]

Looking at the earliest T_w delay ($T_w = 100$ fs) displayed in Fig. 3, the 0-1 and 1-2 peaks appear elongated along the diagonal because their widths along the ω_τ axis are smaller than their total widths (observed by looking at the projection of the peak on the ω_m axis). The width of the projection of the 0-1 peak at a particular ω_m onto the ω_τ axis is the "dynamical linewidth."[5,66,67] Because the hydroxyl stretch of HOD is inhomogeneously broadened for small T_w, the resulting band shapes are asymmetric.[5,66,67] As T_w increases (see the T_w panels of Fig. 3), the dynamic linewidths of the 0-1 and 1-2 peaks (projection of ω_m onto the ω_τ axis) broaden. By $T_w = 1600$ fs, the width of the 0-1 peak along the ω_τ axis has grown almost to the asymptotic value, that is, the width when all possible frequencies have been sampled because of complete structural randomization. Changes in the dynamical linewidth report the spectral diffusion dynamics. The dynamical linewidth can be measured by selecting a cross sectional cut of the 0-1 peak at a particular ω_m value and projecting it onto the ω_τ axis. The horizontal dashed line shown in the $T_w = 100$ fs panel of Fig. 3 illustrates such a cut at the approximate center of the hydroxyl stretch peak (2500

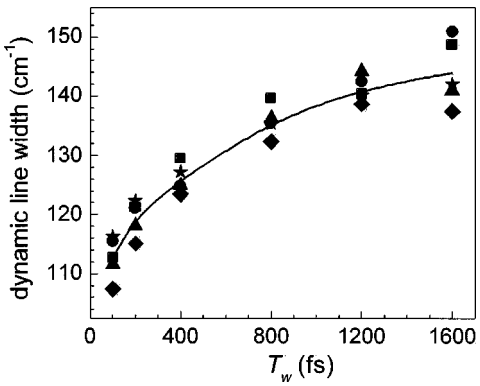

FIG. 4. The dynamic linewidths of 2500 cm^{-1} slices that were extracted from five independent sets of vibrational echo correlation spectra (see text for details). Five distinct experiments were performed over a period of several months. Each experiment produced one correlation spectrum at each T_w point. The triangles report the dynamic linewidths obtained from the correlation spectra that are presented in Fig. 3. The black curve is a guide to the eye. Different bandwidths (pulse durations) were used in the experiments, which prevents the five sets of data from being averaged together without first correcting for the different pulse durations.

cm^{-1}). The dynamical line measured in the correlation spectra of HOD is narrow when spectral diffusion has not randomized the distribution of hydroxyl stretch frequencies. As spectral diffusion occurs, the dynamical linewidth broadens, which is captured by the increased width of the cut at 2500 cm^{-1}.[5,19]

Excited state relaxation occurs with a wavelength independent 1.45 ps time constant as T_w increases,[55] which reduces the amplitude of the emitted vibrational echo and produces photoproducts that are spectrally distinct in about 2 ps (see above). Consequently, the signal amplitudes of the data displayed in Fig. 3 decay by a factor of ~3 from 100 to 1600 fs. The data in Fig. 3 have been normalized to the amplitude of the 0-1 peak, which obscures the decay. Because we want to study the hydrogen bond dynamics of equilibrium water, not the photoproducts caused by hydrogen bond breaking following vibrational relaxation, we restrict our observation window to <2 ps. Studying OD in H_2O enables us to examine the equilibrium hydrogen bond dynamics of water over a time window that is approximately twice to that of investigations of OH in D_2O.[17,18] OH in D_2O has a substantially shorter lifetime (~0.7 ps).[56,57] Therefore, photoproducts will be generated on a shorter time scale. Furthermore, the vibrational quantum of energy deposited upon vibrational relaxation is substantially larger for a OH stretch and may lead to a larger photoproduct contribution. Photoproduct generation has not been taken into account in the analysis of vibrational echo data for the OH in D_2O system.[17,18]

The cuts at 2500 cm^{-1} are well described by a Gaussian line shape. We fit the cuts at $\omega_m = 2500\,cm^{-1}$ from the correlation spectra presented in Fig. 3 to extract the full width at half maximum (FWHM) and to quantify the change in the dynamical line as a function of T_w delay. The dynamical linewidths extracted from the data in Fig. 3 are the triangles in Fig. 4. The dynamic linewidths display the same trend as the correlation spectra, small width at $T_w = 100$ fs (~112 cm^{-1}), which increases with T_w delay (~143 cm^{-1} by 1600 fs). Four other sets of dynamic linewidths are presented in Fig. 4 (circles, squares, diamonds, and stars) that were extracted from additional sets of correlation spectra. The solid black line is a guide to the eye.

The method we used to extract the dynamics of water from the correlation spectra, selection of cuts at 2500 cm^{-1}, has two distinct advantages that enable the most accurate measurement of the structural evolution of water. First, the method can extract the dynamics of water without interference from the 1-2 transition. Because we accurately determined the anharmonicity (Sec. III A 1), it was possible to assess the contribution of the 1-2 transition at 2500 cm^{-1}. It was determined that the contribution is negligible. Consequently, it is unnecessary to remove its influence[5] when fitting the slice at 2500 cm^{-1} to obtain the dynamic linewidth of the 0-1 transition. (Nonetheless, the 1-2 transition is included in the theoretical calculations presented below.) Recent investigations of water dynamics[17,18] were unable to selectively measure the dynamics of the 0-1 transition because the investigators used frequency integrated two[18] and three[17] pulse vibrational echo measurements. The inclusion in data of the 1-2 transition, which can have different dynamics, complicates the analysis and may influence the FTCF determined from such data.

The second advantage of the method is that it selects the central frequency of the 0-1 transition, which facilitates comparison with theoretical simulations of water (Sec. III B). In a recent vibrational echo correlation spectroscopy study of water, it was found that the dynamical line shapes measured at different wavelengths across the OD hydroxyl stretch band of HOD in water vary in width at very short T_w delays.[19] The wavelength dependence indicated that different water molecules experience fluctuations that are specific to their hydrogen bonded configuration. By $T_w \sim 400$ fs, the dynamical linewidths become wavelength independent because the very local structures of different hydrogen bonded configurations are randomized.[19] The frequency dependence of the dynamical linewidth cannot be described by the diagrammatic perturbation theory treatment used to simulate the vibrational echo correlation spectra because of the Gaussian approximation that is implicit in the theory.[41,52,62,63] The method we use mitigates this short coming by selecting the central frequency of the 0-1 transition to represent the dynamics of the entire distribution. The method is rigorously correct for the longer time scale dynamics ($T_w > 400$ fs), and the oppositely signed errors at the earlier T_w delays cancel because we use the central frequency.

Part of the spread in the different data sets shown in Fig. 4 is not random error. Differences arise if the data sets are collected with different pulse bandwidths. To reduce the error bars in the determination of the time evolution of the dynamic linewidths, a method is needed to combine the results of the five experiments into a single composite set of data. However, the groups of data presented in Fig. 4 cannot be averaged together without first correcting the dynamic linewidths from each experiment for the influence of the corresponding laser pulse bandwidths. During each measurement, the laser pulses were transform limited and did not vary while the data were collected. However, different ex-

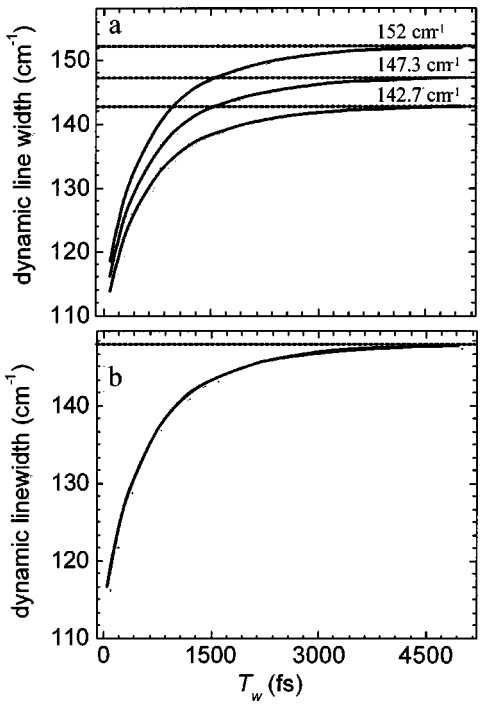

FIG. 5. (a) Dynamic linewidths from calculated vibrational echo correlation spectra that used different pulse durations (45, 51, and 57 fs, top to bottom). The linewidths rise to different limiting values because the bandwidth affects the asymptotic limit. The spread in asymptotic limits is the reason that the data displayed in Fig. 4 cannot simply be averaged together. (b) The three sets of dynamic linewidths displayed in Fig. 5(a) but recast to have the average pulse duration (51 fs) using the correction procedure developed in the Appendix. The exact superposition of all three curves demonstrates that the procedure corrects the experimental data for the influence of finite pulse durations.

periments employed laser pulses that varied in duration from 45 to 57 fs. The pulse durations were precisely determined by measuring the cross correlation of the three laser pulses in a sample that gave a purely nonresonant signal.[40]

To illustrate the importance of correcting the data sets, we calculated correlation spectra with 45, 51, and 57 fs pulse durations to simulate the effect of the actual laser pulses. We employed time dependent diagrammatic perturbation theory to obtain the full third-order nonlinear material response including finite pulse durations.[41,52,62,63] The implementation has been described in detail elsewhere.[5] Briefly, the diagrammatic treatment uses a FTCF as input to obtain the response functions employed in the calculations of the correlation spectra. The FTCF used as input to the calculations was the experimentally determined FTCF that describes the equilibrium fluctuations of water (the method by which the FTCF was obtained from the data is described below). The FTCF was scaled to reproduce the linear linewidth observed from the linear absorption spectrum (FWHM=170 cm^{-1}).[5] Three groups of correlation spectra were calculated using the same FTCF. Only the pulse durations varied between the sets. The top, middle, and bottom curves in Fig. 5(a) display the dynamic linewidths obtained from the correlation spectra calculated with 45, 51, and 57 fs pulse durations, respectively. The dynamic linewidths were acquired from Gaussian fits to the 2500 cm^{-1} cuts out of the correlation spectra. T_w delays were calculated from 0.1 to 5 ps, which is sufficient time delay for spectral diffusion to be complete. The dynamic linewidths are narrow at small T_w delays and grow to their asymptotic limits by 5 ps for all three groups. The asymptotic limits corresponding to the 45, 51, and 57 fs pulse durations are displayed as the dotted lines in Fig. 5(a). The asymptotic line widths for the three pulse durations are 152, 147.3, and 142.7 cm^{-1}, respectively. For infinite pulse bandwidth, the asymptotic limit is the linear absorption linewidth. However, for finite bandwidth pulses, the asymptotic linewidth is reduced because the entire absorption spectrum is not excited equally. The laser pulse durations used in the simulations reflect the range of pulse durations used in the experiment. Consequently, the asymptotic limit of the data presented in Fig. 4 also varies between 152.0 and 142.7 cm^{-1}. The dynamic linewidth in the experiment does not reach its asymptotic limit within our time window of observation ($T_w=1600$ fs), which is limited by the appearance of the broken hydrogen bond photoproducts (see above discussion). Consequently, we rely on precise knowledge of the limit *a priori* in fitting the data. Given that the dynamic linewidth varies by 35 cm^{-1} over the T_w range in the data sets, the variance in the asymptotic limit due to different pulse durations produces substantial shifts not only in the asymptotic limit, but in the entire T_w dependent curve. The variation is $\pm 15\%$ for the range of pulse durations used. This produces unacceptable apparent errors in the data.

To address this issue, we developed a procedure to correct the dynamic linewidths for the influence of finite pulse durations. Expressions are provided in the Appendix describing the dependence of the correlation spectra on the laser pulse bandwidth. From this dependence, the correction procedure is developed. The correction procedure was applied to the simulated dynamic linewidths displayed in Fig. 5(a). The linewidths calculated with 45 and 57 fs pulses are recast into the median pulse duration 51 fs. Figure 5(b) displays the three sets of calculated dynamic linewidths after the correction procedure was applied [see Eqs. (A12) and (A13)]. The sets are indistinguishable. What appears as a single curve in Fig. 5(b) is the superposition of three identical curves. The comparison demonstrates that the effects of finite-bandwidth pulses on the dynamic line widths are precisely described by Eqs. (A12) and (A13), and that the procedure described in the Appendix can be used to combine data sets taken with different bandwidths.

Having verified the accuracy of the correction procedure, we applied the method to the five sets of experimental dynamical linewidths presented in Fig. 4. After correction for the differences in bandwidth, the averaged data give the points with error bars shown in Fig. 6. The scatter in the data at each T_w point yields error bars, defined as one standard deviation ± 2.5 cm^{-1}. The dynamic linewidth data climb towards a well-defined asymptotic limit of 147.3 cm^{-1} (determined from the pulse duration and the linear linewidth). The dynamic width in Fig. 6 approaches, but does not reach the asymptotic limit by $T_w=1600$ fs.

Before analyzing the data presented in Fig. 6 in detail, it is necessary to determine the influence of photoproduct generation on the experimentally determined dynamic linewidths. The real dynamic line shape $G_{\mathrm{dyn}}(\omega_\tau)$, which would

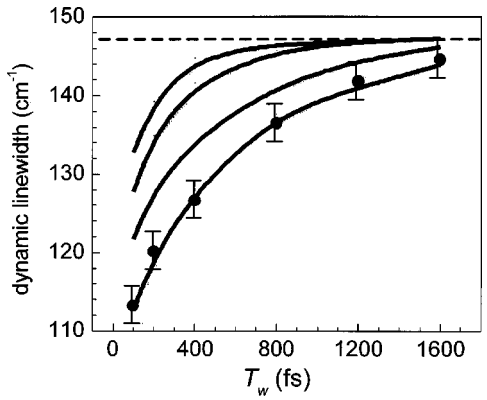

FIG. 6. Comparison of the dynamical linewidths of the simulated and experimental correlation spectra obtained from the $\omega_m = 2500\ \mathrm{cm}^{-1}$ slices. The experimental data appear as circles with error bars. The horizontal line at 147.3 cm^{-1} is the long time asymptotic linewidth. The top curve is from the TIP4P model and the next lower curve is from the SPC/E model. Both models have reached the asymptotic limit by 1.6 ps. Compared to the data, both models have too much amplitude at short time and the long time components are too fast. The third from top curve is from the SPC-FQ model, which is a polarizable water model. The SPC-FQ model displays considerably better agreement with the experimental dynamics that the TIP4P or SPC/E models. Most importantly, the SPC-FQ model has not reached the asymptotic limit by 1.6 ps. The curve through the data is from a fit to the data obtained by varying the parameters of a triexponential trial FTCF until the dynamical linewidths best fit the data. The experimental FTCF provides a fit to the data within experimental error.

be measured in the absence of the photoproduct, can be calculated from the measured dynamic line shape $G_m(\omega_\tau)$ according to the following expression:

$$G_{\mathrm{dyn}}(\omega_\tau) = (1-A)^{-1}[G_m(\omega_\tau) - AG_{\mathrm{pp}}(\omega_\tau)]. \quad (4)$$

$G_{\mathrm{pp}}(\omega_\tau)$ is the ω_τ dependent line shape corresponding to the photoproduct and A is the fractional contribution to the measured signal from the photoproduct. The influence of photoproducts on the correlation spectra has been discussed in detail in a recent vibrational echo correlation spectroscopy study of methanol oligomers.[45,48,68,69] It was demonstrated that the photoproduct line shape along the ω_τ axis is the asymptotic line shape when it is formed without fine frequency correlation with the initially excited hydroxyl distribution.[69] When fine frequency correlation exists between a photoproduct and its parent molecule that was initially excited, the photoproduct retains a detailed memory of the parent frequency within the inhomogeneous hydroxyl stretch distribution. The dynamical linewidth of the photoproduct is narrow, just like the parent dynamical linewidth was prior to hydrogen bond breaking. This fine frequency correlation, which was observed in methanol oligomers in CCl_4,[69] does not exist in water. Consequently, the dynamic linewidth of the photoproduct is the asymptotic linewidth for the total hydroxyl distribution (147.3 cm^{-1}).

The contribution of the photoproduct to the vibrational echo correlation spectrum signal amplitude as a function of T_w delay was determined independently from ultrafast infrared transient absorption experiments (3%, 8%, and 15% at $T_w = 800$, 1200, and 1600 fs, see Fig. 2). Solving Eq. (4) for each T_w point displayed in Fig. 6, we find that the photoproduct produces an increase of $\leqslant 0.5\ \mathrm{cm}^{-1}$ to the true dynamic linewidth at all T_w delays. This quantity is insignificant compared to the measured linewidths that have error bars of $\pm 2.5\ \mathrm{cm}^{-1}$. The photoproduct adds negligibly to the measured widths because the vibrational lifetime (1.45 ps) is comparable to the longest decay component in the frequency fluctuations (1.4 ps, see discussion that follows). The frequency fluctuations have nearly randomized the distribution of hydroxyl stretches before the photoproduct contributes significantly to the signal. Consequently, the dynamic linewidths reported in Fig. 6 do not need to be corrected for the contribution from the photoproduct.

We note that the time dependent contribution from hydrogen bond breaking photoproducts was not considered in other recent reports of water FTCFs,[17,18] which interrogated the OH stretch of HOD in D_2O. Recent mixed electronic structure and molecular dynamics simulations of water have demonstrated that the frequency fluctuations in D_2O are nearly identical to those in water.[54] Yet, the vibrational lifetime of the OH stretch of HOD in D_2O is half the duration compared to the OD stretch of HOD in water. Consequently, the photoproducts will contribute much earlier in the studies involving the OH stretch.[17,18] In addition, a larger quantum of energy is deposited upon vibrational relaxation, which could result in increased photoproduct generation through hydrogen bond breaking. Therefore, photoproduct generation might influence the reported FTCFs.

B. Comparisons of experimental results and theoretical models

The data presented above reflect the equilibrium dynamics of water. They are free of artifacts resulting from excited state (1-2 transition) contributions, photoproduct contamination, and finite pulse duration effects. We now compare the water dynamics obtained experimentally with the dynamics that are predicted by three models of water: TIP4P,[50] SPC/E,[51] and SPC-FQ.[53] The comparisons provide a context for discussing the data and rigorously test the accuracy with which these three models predict the dynamics of water.

The following four step sequence[5] is used to compare the theoretically derived dynamics with the experimental results.

(1) A particular water model simulation is implemented.

(2) The FTCF for a given model of water is generated from methods that involve electronic structure (ES) calculations and classical molecular dynamic (MD) simulations.

(3) We calculate the vibrational echo correlation spectra from the FTCF using time dependent diagrammatic perturbation theory.[5,41,52,62,63]

(4) We extract the T_w dependence of the dynamical linewidth and compare to the experimental data.

The mixed ES/MD method used to calculate the normalized FTCF for the OD stretch of HOD in H_2O (Refs. 49 and 54) is based on *ab initio* electronic structure calculations of clusters of water molecules. First, configurations of molecules are generated from a given classical molecular dynamics simulation of the HOD/H_2O system. Then a representative set of HOD$(H_2O)_n$ clusters are extracted from the simulation. For each cluster a series of *ab initio* calculations (using density functional theory) are performed for different

TABLE I. TFCF parameters [see Eq. (5)].

TFCF	Δ_0 (rad/ps) (%)	τ_0 (ps)	Δ_1 (rad/ps) (%)	τ_1 (ps)	Δ_2 (rad/ps) (%)	τ_2 (ps)
Fit	10.1 (41)	0.048	3.8(15)	0.4	10.9(44)	1.4
SPC-FQ	12.0 (44)	0.048	5.5(20)	0.35	9.8(36)	1.45
SPC/E	12.1 (42)	0.031	9.0(32)	0.28	7.4(26)	0.98
TIP4P	15.2 (55)	0.032	10.2(37)	0.34	2.2 (8)	0.90

values of the OD stretch coordinate, and in doing so an anharmonic potential curve that leads to a 0-1 OD transition frequency for the HOD molecule in that cluster is generated. From looking at a hundred or so clusters, it was determined that there is a linear correlation between the OD frequency and the component of the electric field from the H_2O molecules on the D atom in the direction of the OD bond vector (correlation coefficient=0.9). Assuming this same linear correlation holds for the full liquid, the normalized FTCF simply becomes the normalized electric field time correlation function. The latter can be generated easily from a completely classical molecular dynamics simulation. Using this ES/MD method,[49,54] the simulation was actually performed on the neat H_2O system, which provides much better statistics by averaging over all molecules. It was determined that this change makes a negligible difference.[54] With this method, it is very easy to examine various models of water. In this paper we report comparisons to the data for the OD stretch of TIP4P,[50] SPC/E,[51] and SPC-FQ[53] HOD in H_2O.

The FTCFs obtained from the ES/MD simulations are fit with exponential functions to obtain an analytical representation. The numerical FTCFs can be represented exceedingly well by the sum of three exponentials.[5] Calculations with the numerical FTCFs generated by the simulations produced indistinguishable correlation spectra from those generated with the exponential fits. However, considerable calculation time was saved using the analytical forms. These functions have the form

$$C(t)=\Delta_0^2\exp(-t/\tau_0)+\Delta_1^2\exp(-t/\tau_1)+\Delta_2^2\exp(-t/\tau_2). \quad (5)$$

While the time constants in Eq. (5) were obtained directly from the simulations, the magnitudes of the prefactors were multiplied by a constant to reproduce the full width at half maximum of the experimentally measured linear absorption spectrum (170 cm^{-1}).[5] We will henceforth refer to the triexponential fits as the FTCFs. The parameters of the exponential functions describing the FTCFs for each water model are displayed in Table I. Additionally, parameters describing the FTCF obtained from fitting the data are provided in the table. The method by which this FTCF was obtained is discussed below.

We calculated theoretical vibrational echo correlation spectra from the appropriately scaled FTCFs (Step 3, see above) using diagrammatic perturbation theory to obtain the third-order nonlinear material response, including finite pulse durations.[5,41,52,62,63] The calculations included all contributing pathways to the 0-1 and 1-2 peaks.[5,41,52,62,63] We approximated the frequency fluctuations of the 1-2 transition as being the same as the 0-1 transition (harmonic approximation). This assumption allowed us to use the same FTCF to describe the 0-1 and 1-2 transitions and caused the two peaks to have the same dynamic linewidths and total widths.

Having input the experimentally determined anharmonicity (162 cm^{-1}, see above), the calculations demonstrated that within the harmonic approximation, the 1-2 peak does not contribute significantly at 2500 cm^{-1}. Therefore, the T_w dependent dynamical linewidths of the 0-1 transition in the theoretical correlation spectra are accurately measured by fitting slices at 2500 cm^{-1} with Gaussian line shapes. The same analysis scheme was used for the experimental correlation spectra. Although the harmonic approximation may not be strictly valid for water, the contribution of the 1-2 peak at 2500 cm^{-1} is so small that employing the harmonic approximation should have a negligible influence on the dynamic linewidth. In any event, any contribution from the 1-2 transition is included in both the measurement and the calculations.

Correlation spectra were calculated for each water model at six T_w delays coinciding with the experimental data (T_w = 100, 200, 400, 800, 1200, and 1600 fs) and at T_w=5 ps (to insure that the calculation reached the correct asymptotic limit). Representative theoretical correlation spectra for the SPC/E model of water have been presented previously.[5] Slices of the correlation spectra were selected at 2500 cm^{-1} and fit with Gaussian line shapes to quantify their widths. The Gaussian function accurately fit the slice and provided a measure of the dynamic linewidth.

The dynamic linewidths calculated from the TIP4P (top curve),[50] SPC/E (second from top),[51] and SPC-FQ (third from top)[53] models of water are displayed as a function of T_w delay in Fig. 6. The dynamic linewidths calculated for the TIP4P and SPC/E models were reported previously[5] and are included here for comparison. The data are displayed in Fig. 6 as the filled circles with error bars. The dashed line at 147.3 cm^{-1} represents the asymptotic dynamic linewidth for the 51 fs pulse duration (see Sec. III A 3). The same pulse duration was used in the diagrammatic perturbation theory calculations. The line through the composite data is a fit, which yielded the experimental FTCF (see discussion that follows). The dynamic linewidths calculated from the water model FTCFs and the experimental FTCF, all ascend (at sufficiently long T_w delay) to the same asymptotic value because the FTCFs were scaled to reproduce the linear linewidth (170 cm^{-1}).[5]

The dynamic linewidths extracted from the calculated correlation spectra display the same trend as the experimental data. The widths are narrow at early T_w and increase toward the asymptotic linewidth with increasing T_w delay because spectral diffusion randomizes the frequencies in the

hydroxyl stretch peak. The rate of increase in the dynamic linewidth for each model is determined by the corresponding FTCF. The triexponential fit parameters corresponding to each water model are displayed in Table I. The comparison in Fig. 6 demonstrates that the TIP4P and SPC/E water models describe the dynamics of water that are reflected by the frequency fluctuations of the hydroxyl (OD) stretch relatively poorly.[5] The dynamic linewidths predicted by both models are much too large at $T_w = 100$ fs and increase to the asymptotic linewidth by 1600 fs, considerably faster than the composite data. These models overemphasize the fast fluctuations and do not contain a slow enough component to account for the slowest fluctuations.

The third water model simulated in this work SPC-FQ,[53] better describes the dynamics of water compared to the TIP4P and SPC/E models. The dynamic linewidth calculated from the SPC-FQ model at $T_w = 100$ fs deviates only ~ 8 cm^{-1} from the experimental dynamic linewidth measured at the same T_w delay. In contrast, the dynamic linewidth calculated from the TIP4P and SPC/E models deviated ~ 20 and ~ 14 cm^{-1}, respectively, at $T_w = 100$ fs. Of greater significance is the fact that the dynamic linewidth calculated from the SPC-FQ model increases more slowly towards and does not reach the asymptotic limit by $T_w = 1600$ fs, in contrast to the TIP4P and SPC/E models. These differences indicate that the SPC-FQ model more accurately describes the frequency fluctuations of water.

Based on the results from the water model calculated FTCFs, a triexponential form for the FTCF was used to fit the experimental data. We begin by entering a triexponential function as the FTCF into the full third-order material response calculation.[5,41,52,62,63] As output, simulated correlation spectra are generated. A slice at 2500 cm^{-1} is used to obtain the time dependent dynamic linewidths for each T_w. This output is compared with the experimental data. The process is iteratively repeated, and the parameters in the FTCF are varied until the dynamical linewidths obtained from the simulated correlation spectra produce the best least squares fit to the experimental data.

The triexponential function describing the experimental FTCF was constrained to be consistent with other complementary experiments and calculations to obtain the greatest confidence in the parameters. Constraint of the initial magnitude of the FTCF was achieved by fitting the linear absorption line shape calculated from the FTCF to the absorption spectrum.[5] The FTCF reproduces the long time asymptotic value of the dynamic line width 147.3 cm^{-1}, which results when 51 fs pulses are used. This procedure also causes the pre-exponential factor Δ_i^2 of one the exponential components to be dependent on the other two. As a result, only two of the three Δ's were varied independently in the fitting procedure. The amplitudes of the Δ's in Table I reflect the appropriate initial magnitude to reproduce the linear line shape. In all three simulations of the FTCF, the fastest component is motionally narrowed, that is, $\Delta_0 \tau_0 < 1$. In this case, this component contributes an exponential decay in the time domain to the total time domain vibrational echo decay with decay rate $\Delta_0^2 \tau_0$. Therefore, τ_0 and Δ_0 are not independent. The SPC-FQ provided the FTCF that produced the T_w dependent linewidths that are closest to the data. Therefore, $\tau_0 = 48$ fs was fixed and only Δ_0 was varied. Three pulse photon echo peak shift measurements were made on the intermediate time scale and gave $\tau_1 = 400$ fs.[5] This measurement provided the intermediate time constant because once the FTCF has decayed sufficiently, the vibrational echo peak shift as a function of T_w gives the time dependence of the FTCF.[70–73] Therefore, in the fitting procedure, three parameters were allowed to vary independently; the preexponential factors of two of the components and the time constant of the slowest component.

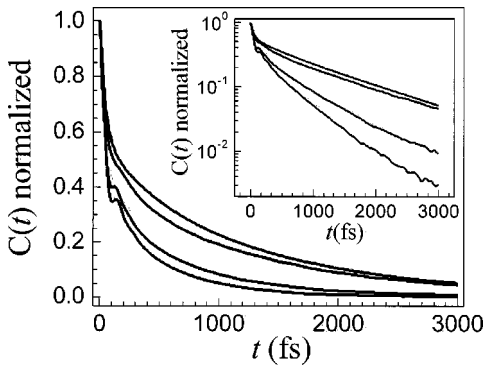

FIG. 7. Comparison of the FTCF corresponding to the TIP4P, (bottom curve) SPC/E, (second from bottom) SPC-FQ (third from bottom) models and the experimental FTCF (top curve). The inset displays the same FTCFs on a semi-long plot with the curves in the same order as in the main portion of the figure. The SPC-FQ model gives an FTCF that is remarkably close to the experimental FTCF, and it is far superior to the other two.

The line through the data points in Fig. 6 is the result of the fitting procedure. Because the error bars on the measured points are small, the fit is highly constrained. In contrast to the dynamical linewidths produced from the water models, the dynamic linewidth obtained from the experimental FTCF has the correct value at $T_w = 100$ fs. The calculated widths pass through the data points within experimental error. The dynamical linewidth at $T_w = 1600$ fs has not reached the asymptotic value and approaches it relatively slowly.

The normalized FTCF that provided the best fit to the experimental dynamical linewidths is displayed in Fig. 7 (top curve) in addition to the FTCFs for the TIP4P (bottom), the SPC/E (second from bottom), and the SPC-FQ (third from bottom) water models. The triexponential parameters for each FTCF are displayed in Table I. The fit through the experimental data has a 1.4 ps time constant for the slowest component that comprises 44% of the decay. We estimate upper and lower bounds of ± 0.2 ps based on a factor of 2 increase in the sum of the squares of the residuals.

The inset in Fig. 7 displays the FTCFs in the same order as the main portion of the figure but on a semilog scale to emphasize the behavior at long time. It is clear from both the main portion of the figure and the inset that the SPC-FQ model comes much closer to reproducing the data than the other two models. In fact, it is remarkable how close the experimentally derived FTCF and the SPC-FQ FTCFs are. The fast components of the theoretical FTCFs comprise approximately half of the total decay amplitude. This feature is reproduced by the experimentally derived FTCF, even

though this amplitude was allowed to vary independently in the fit. The long time behavior of the TIP4P and SPC/E models compared to the experimental FTCF are consistent with their behavior reported previously.[5] The TIP4P model essentially misses the slow component completely. The SPC/E model does better but overestimates the magnitude of the intermediate and underestimates the magnitude of the slow components. In addition, the SPC/E model underestimates the time scale of the slow component. Comparing the experimental and SPC-FQFTCFs demonstrates that this model more accurately describes the fluctuations of water than the TIP4P or SPC/E models. In fact, the time scale of SPC-FQs slow component (1.45 ps) is identical, within experimental error, to the measured value (1.4 ps, see above discussion). The only difference between the experimentally derived FTCF and the SPC-FQFTCF are relatively small differences in the amplitudes of the components (see Table I). It is interesting to note that we scaled the FTCFs derived from the three water models and from the experiment to fit the OD stretch linear absorption spectrum so that the dynamic linewidths (see Fig. 6) would ascend to the same asymptotic value. However, the FTCF generated from the SPC-FQ model accurately predicted the linear linewidth within a few percent without scaling, which further supports the conclusion that the SPC-FQ model more accurately describes the dynamics of water.

The time dependent structural evolution that is obtained from simulations, enables us to correlate specific motions of water with components of the FTCF. The decay components of the TIP4P FTCF have been assigned for the OH stretch of the HOD/D_2O system.[2–4,74,75] The fast component was assigned to hindered translational motion of the hydrogen bonds (stretching of the hydrogen bond length coordinate). There is also a small contribution from hydrogen bond bending.[2–4,76] This assignment was based on the observation of a shallow oscillation of about one cycle in the FTCF with a period that corresponds to the estimated period of hindered translational motion.[3] The oscillation is also present with varying amplitudes in the FTCFs obtained from simulations for the HOD/H_2O system (see Fig. 7).[49] The SPC-FQFTCF does not display the oscillation but exhibits inflections at the period of the hindered translational motion. It is safe to assume that the same physical interpretation holds for the HOD/H_2O system. Therefore, the fast component of the FTCFs mainly reflects the time scale of fluctuations in the hydrogen bond length coordinate. The fact that the oscillation is damped nearly to zero in the SPC-FQ FTCF indicates that it is essentially overdamped in this model while it is just barely underdamped in the other two models. It should be noted that we simulated vibrational echo correlation spectroscopy and vibrational echo peak shift experiments with 50 fs pulse durations using the TIP4P FTCF, which shows the most prominent indication of an oscillation and determined that the oscillation cannot be observed experimentally. The shallowness of the oscillation and the convolution with the pulses eliminate any trace of the oscillation in the data. Using the actual TIP4P FTCF or the triexponential fit that does not have an oscillation produces identical calculated correlation spectra.

The slower portion of the FTCF calculated for the HOD/D_2O system has been assigned to the influence of hydrogen bond breaking and formation. This assignment was based on the similarity in the time constants between the slow component of the FTCF and that of the hydrogen bond population correlation function and from examining the frequency distributions for hydrogen bonded and nonhydrogen bonded oscillators.[3,4,75,76] This correlation function depends on the rate of hydrogen bond formation *and* breaking. In the simulations, the definition of the existence of a hydrogen bond is in terms of the oxygen-oxygen distance, the oxygen-hydrogen distance, and the angles involved.[77] Again, this identification of the slow component with hydrogen bond equilibration should also hold for the HOD in H_2O system. The experimental results demonstrate the time scales obtained from the TIP4P and SPC/E water models are too fast and contain too little amplitude to describe the dynamics that we observe in water. However, the SPC-FQ model provides a much more accurate description of the dynamics of hydrogen bond equilibration (making and breaking). Recent broadband transient absorption experiments that examine hydrogen bond equilibration, which is observed to be complete in 5 ps,[55] support the assignment of the slowest component of the FTCF as the hydrogen bond equilibration time.

It seems likely that the SPC-FQ model more accurately captures the structural fluctuations of water because it contains a method for including water polarizability through the influence of water molecules on each other.[53] Unlike the TIP4P and SPC/E models, the partial charges in the SPC-FQ model are not fixed but rather change position in response to the electric fields produced by the other water molecules. This feature is absent in the TIP4P and SPC/E models.[50,51] The polarizability term introduces collective effects into the intermolecular pair potential between neighboring water molecules. The partial charges assigned to a particular pair of water molecules are influenced by the collective electric field that results from the water molecules surrounding the pair. The partial charges in part determine the intermolecular pair potential that governs the behavior of the water pair. The intermolecular distance and bond angles are affected by the intermolecular pair potential. This collective effect produces the ~50% slower dynamics in the SPC-FQ model compared with the non-polarizable models.[54,78] The collective effect also enhances the magnitude of the slower fluctuations in the SPC-FQ model (see Table I). The improved description of the dynamics in water that resulted from the inclusion of the polarizability term suggests that collective effects dominate the slower time scale motions of water. It will be important to determine if other polarizable water models also do a superior job of reproducing the experimental data.

IV. CONCLUDING REMARKS

Water dynamics were studied using ultrafast heterodyne detected multidimensional stimulated vibrational echo correlation spectroscopy with full phase information. Five completely independent sets of experiments were performed over a period of several months to establish the reproducibility and reduce the error bars in the measurement of the water dynamics. A procedure was described for accounting for the

influence of finite pulse durations on the vibrational echo correlation spectra. Additional experiments were performed to provide highly accurate measurement of the vibrational anharmonicity (162 cm^{-1}) and excited state lifetime for the OD hydroxyl stretch (1.45 ps). Following excited state relaxation, hydrogen bonds break in water and photoproducts form. Infrared pump-probe experiments were employed to determine the buildup time for the photoproducts (~2 ps). Therefore, the dynamic linewidths were collected for times shorter than 2 ps to avoid significant contamination from the photoproduct. Careful measurement of the photoproduct contribution at all T_ws proved that the photoproduct contribution was insignificant at all T_w delays that were reported. Therefore, the vibrational echo correlation spectra provide information free from the influence of photoproducts and without complication from the dynamics of the 1-2 transition. From these data, an accurate picture of water dynamics emerged.

The dynamic linewidth, measured as a horizontal cut at 2500 cm^{-1} across the two-dimensional 0-1 peak of the correlation spectra (see Fig. 3), displays the time evolving frequency distribution sampled by water molecules as a function of T_w delay. Analysis of the dynamic linewidths demonstrates that the frequency fluctuations of water are not complete by 2 ps. Fitting the T_w dependent dynamic linewidths using time dependent diagrammatic perturbation theory provided the experimental FTCF.

Electronic structure calculations and molecular dynamics simulations gave the FTCF for the polarizable SPC-FQ water model as well as two nonpolarizable models (TIP4P and SPC/E). These FTCFs were used to calculate the experimental observables, which were compared to the data in Fig. 6. In Fig. 7, the calculated FTCFs and the experimental FTCF are compared. The SPC-FQ FTCF is very close to the experimental FTCF (see Fig. 7 and Table I), while the other two calculated FTCFs have substantial deviations from experiment. The SPC-FQ water model is ''polarizable'' while TIP4P and SPC/E models are not. The polarizability aspect of the SPC-FQ model may be responsible for its accuracy.

The simulations provide qualitative insights into the physical meaning of the dynamics measured on different time scales. The very short time dynamics are associated with hydrogen bond length fluctuations. The longest time scale observed in the measurements is associated with hydrogen bond equilibration, the making and breaking of hydrogen bonds. The experimental FTCFs slow component comprized ~44% of the decay with a time constant of 1.4 ps. The slow component of the FTCF derived from the SPC-FQ model contained a 1.45 ps time constant that comprised ~36% of the decay. The accurate description of hydrogen bond equilibration is most important for describing water as a chemical and biological agent because it is on this time scale that the complex hydrogen bond network structure undergoes global evolution.

ACKNOWLEDGMENTS

J.B.A., T.S., K.K., and M.D.F. would like to thank AFOSR (Grant No. F49620-01-1-0018) and NIH (Grant No. 2R01GM061137-05) for support of this research and additional support provided by NSF DMR (Grant No. DMR-0332692). C.P.L. and J.L.S. would like to thank NSF (Grant Nos. CHE-9816235 and CHE-0132538) for support of this research. S.A.C. acknowledges the support of a Ruth L. Kirschstein National Research Service Award administered through NIH.

APPENDIX: INFLUENCE OF FINITE PULSE DURATIONS AND COMBINING DATA SETS

Finite-duration laser pulses influence the data collected in a vibrational echo experiment through a time domain (time ordered) convolution between the ideal signal (which would be observed with infinitely short pulses) and the pulses' temporal envelopes. Vibrational echo correlation spectroscopy is a time-domain experiment. The two frequency axes in the correlation spectra, denoted as $S_{\mathrm{VECS}}(\omega_\tau, T_w, \omega_m)$, result from Fourier transformation of the τ and τ_s time dimensions, respectively,

$$S_{\mathrm{VECS}}(\omega_\tau, T_w, \omega_m) = 2\,\mathrm{Re}\int_{-\infty}^{\infty} d\tau \exp(i\omega_\tau \tau) \times \int_{-\infty}^{\infty} d\tau_s \exp(i\omega_m \tau_s) P^{(3)}(\tau, T_w, \tau_s) \times \int_{-\infty}^{\infty} d\tau_s \exp(i\omega_m \tau_s) E^*_{\mathrm{LO}}(\tau_s). \quad \text{(A1)}$$

The product of Fourier transforms along the τ_s dimension results from the hererodyne amplified signal [Eq. (1)] and occurs experimentally in the monochromator. The τ dimension is Fourier transformed numerically after the data are collected. $P^{(3)}(\tau, T_w, \tau_s)$ is the third-order polarization in the sample that emits the vibrational echo, which is induced by interaction with the three laser pulses. τ is the time separation between the first and second laser pulses, and τ_s is the time following the third laser pulse, during which the echo is emitted. By resolving the phase of the vibrational echo, we selectively measure the absorptive (real) part of the polarization. $E^*_{\mathrm{LO}}(\tau_s)$ is the electric field of the local oscillator,

$$E_{\mathrm{LO}}(t) = e^{i\bar{k}_{\mathrm{LO}}\cdot\vec{r} - i\omega_{\mathrm{LO}}\tau_s} e^{-\tau_s^2/2\sigma^2}, \quad \text{(A2)}$$

which determines the frequency range along the ω_m axis over which the heterodyne cross term can be detected. The influence of finite laser pulse duration on the polarization in the sample is described by the following time ordered integral:[5,41,52,62,63]

$$P^{(3)}(\tau, T_w, \tau_s) = \int_0^{\infty}\int_0^{\infty}\int_0^{\infty} \sum_i R_i(t_3, t_2, t_1) \times E_1^*(\tau_s + \tau + T_w - t_3 - t_2 - t_1) \times E_2(\tau_s + T_w - t_3 - t_2) \times E_3(\tau_s - t_3) dt_1 dt_2 dt_3, \quad \text{(A3)}$$

where the E_i are the electric fields of the three laser pulses

$$E_i(t) = e^{i\bar{k}_i\cdot\vec{r} - i\omega_i t} e^{-i^2/2\sigma^2}, \quad \text{(A4)}$$

and the R_i describe the material response of the sample.[5,41,52,62,63]

Because the correlation spectra are displayed in the frequency domain, we re-express Equations (A1) through (A4) purely in the frequency domain as

$$S(\omega_\tau,\omega_{T_w},\omega_m) = \mathrm{IRF}^{+}(\omega_\tau,\omega_{T_w},\omega_m)\sum_i \tilde{R}_i^{+}(\omega_\tau,\omega_{T_w},\omega_m) + \mathrm{IRF}^{-}(\omega_\tau,\omega_{T_w},\omega_m)\sum_i \tilde{R}_i^{-}(\omega_\tau,\omega_{T_w},\omega_m). \quad \text{(A5)}$$

The instrument response function,

$$\mathrm{IRF}^{+}(\omega_\tau,\omega_{T_w},\omega_m) = \exp\left(-\frac{(\omega_\tau+\omega_0)^2}{\sigma_\omega^2}-\frac{(-\omega_\tau+\omega_{T_w}-\omega_0)^2}{\sigma_\omega^2} - \frac{(-\omega_{T_w}+\omega_m-\omega_0)^2}{\sigma_\omega^2}-\frac{(-\omega_m-\omega_0)^2}{\sigma_\omega^2}\right), \quad \text{(A6)}$$

applies to the rephasing quantum pathways $\tilde{R}_i^{+}$ that result when pulse 1 precedes pulses 2 and 3. The converse instrument response function,

$$\mathrm{IRF}^{-}(\omega_\tau,\omega_{T_w},\omega_m) = \exp\left(-\frac{(\omega_\tau+\omega_{T_w}-\omega_0)^2}{\sigma_\omega^2}-\frac{(-\omega_\tau-\omega_0)^2}{\sigma_\omega^2} - \frac{(-\omega_{T_w}+\omega_m-\omega_0)^2}{\sigma_\omega^2}-\frac{(-\omega_m-\omega_0)^2}{\sigma_\omega^2}\right), \quad \text{(A7)}$$

applies to the nonrephasing quantum pathways $\tilde{R}_i^{-}$ that result when pulse 2 precedes pulses 1 and 3. Here, the frequencies ω_τ, ω_{T_w}, and ω_m are Fourier conjugates of the time variables τ, T_w, and τ_s. σ_ω is the standard deviation of the Gaussian fit to the electric field level spectrum of the laser pulses, and ω_0 is the center frequency of the laser pulses. The instrument response function in the frequency domain [Eqs. (A6) and (A7)] contains the influence of the time-ordered integration ever the pulses expressed in Eqs. (A1) and (A3). The vibrational echo response in the frequency domain, expressed as $\Sigma_i \tilde{R}_i^{\pm}(\omega_\tau,\omega_{T_w},\omega_m)$, is the three-dimensional Fourier transform of its time domain equivalent $\Sigma_i R_i(t_3,t_2,t_1)$.[5,41,52,62,63]

From Eq. (A5), the influence of finite pulse duration can simply be divided out of the vibrational echo signal expressed in the frequency domain. However, the vibrational echo signal represented in Eq. (A5) represents the T_w period in the frequency domain, which is counter intuitive. We want the T_w period expressed in the time domain. Unfortunately, the simplicity of the influence of finite pulse duration is lost when the T_w period is expressed in the time domain. For the purpose of correcting the experimental correlation spectra, we address this problem with the assumption that the dynamics in the T_w period are slow compared to the pulse duration. This assumption removes the dependence of the instrument response function on ω_{T_w}. The instrument response function is reduced to a two-dimensional Gaussian line shape depending only on ω_τ and ω_m. Following the above assumption, the dependence on pulse spectrum of the signal in the correlation spectra can be described by the expression

$$S_{\mathrm{VECS}}(\omega_\tau,T_w,\omega_m) = \exp[-(\omega_\tau-\omega_0)^2/2\sigma_i^2] \times \exp[-(\omega_m-\omega_0)^2/2\sigma_i^2]\sum_i \tilde{R}_i^{\pm}(\omega_\tau,T_w,\omega_m), \quad \text{(A8)}$$

where σ_i is the standard deviation of the intensity level laser spectrum. Therefore, dividing the correlation spectra by the intensity level laser spectrum along both frequency axes deconvolves the correlation spectra from the laser pulses and produces the correlation spectrum that would be measured with infinite bandwidth (delta function) pulses.

In the analysis of the correlation spectra presented in the main body, we selected cross sectional cuts of the 0-1 peaks in the correlation spectra at $\omega_m = 2500\,\mathrm{cm}^{-1}$ to describe the dynamic line shapes as a function of T_w delay. Looking at a single ω_m value, the effect on the data of the instrument response function along the ω_m axis reduces to an amplitude factor that does not impact the analysis. Consequently, we can neglect the ω_m dependence of the instrument response function in the following discussion. By fitting the cross sectional cuts of the correlation spectra with Gaussian line shapes, the vibrational echo signals at $\omega_m = 2500\,\mathrm{cm}^{-1}$ are described by the expression

$$S_{\mathrm{VECS}}(\omega_\tau,T_w) = \exp[-(\omega_\tau-\omega_0)^2/2\sigma_{\mathrm{ob}}^2(T_w)], \quad \text{(A9)}$$

where $2.35\sigma_{\mathrm{ob}}(T_w)$ are the FWHM of the Gaussian fits to the dynamic line shapes that are measured as a function of T_w delay (see Fig. 4). Combining Eqs. (A8) and (A9) and evaluating at $\omega_m = 2500\,\mathrm{cm}^{-1}$, the following expression relates the FWHM of the Gaussian fits to the instrument response function and vibrational echo response, $\tilde{R}_{0\text{-}1}^{\pm}(\omega_\tau,T_w)$,

$$\exp[-(\omega_\tau-\omega_0)^2/2\sigma_{\mathrm{ob}}^2(T_w)] = \exp[-(\omega_\tau-\omega_0)^2/2\sigma_i^2]\tilde{R}_{0\text{-}1}^{\pm}(\omega_\tau,T_w). \quad \text{(A10)}$$

Approximating the vibrational echo response as a Gaussian and taking the natural logarithm of Eq. (A10) produces the equality (assuming the laser is centered on the 0-1 transition)

$$1/2\sigma_{\mathrm{ob}}^2(T_w) = 1/2\sigma_i^2 + 1/2\sigma_R^2(T_w), \quad \text{(A11)}$$

where $2.35\sigma_R(T_w)$ are the FWHM of the Gaussian fits to the vibrational echo response that would be observed in the limit of infinite bandwidth laser pulses ($\sigma_i \to \infty$). Solving Eq. (A11) for $\sigma_R(T_w)$, we obtain an expression for the width of the vibrational echo response as a function of T_w delay in terms of the experimentally observed widths, $\sigma_{\mathrm{ob}}(T_w)$, and the width of the intensity level laser spectrum σ_i

$$\sigma_R(T_w) = \sigma_i\sigma_{\mathrm{ob}}(T_w)/\sqrt{\sigma_i^2-\sigma_{\mathrm{ob}}^2(T_w)}. \quad \text{(A12)}$$

Equation (A12) removes the effect of finite pulse bandwidth on the dynamic linewidth measured from $\omega_m = 2500\,\mathrm{cm}^{-1}$

slices that were selected from the correlation spectra. To be consistent with the data presented in Fig. 4, we solve Eq. (A11) for $\sigma_{ob}(T_w)$,

$$\sigma_{ob}(T_w) = \sigma_R(T_w)\sigma_i / \sqrt{\sigma_R^2(T_w) + \sigma_i^2}. \quad \text{(A13)}$$

Substitution of the solutions for $\sigma_R(T_w)$ from Eq. (A12) into Eq. (A13) enables the data to be recast with the average pulse duration used in the experiment (51 fs). It should be noted that the correction scheme presented above is general for all ω_m frequency slices, not just the 2500 cm^{-1} slice.

We note that we used full third-order diagrammatic perturbation theory to calculate the dynamic linewidths displayed in Fig. 5(a), which rigorously calculated the effect of finite-bandwidth pulses. The calculations did not use the simplifying assumption that the dynamics during the T_w period are slow compared to the pulse duration, which we made in the development of Eqs. (A12) and (A13). The fact that the three sets of dynamic line widths displayed in Fig. 5(b) superimpose exactly onto each other demonstrates that our treatment precisely corrected the effects of finite-bandwidth pulses and validates the assumption of slow dynamics compared to the pulse duration during the T_w period. If considerably longer pulses were used, the assumption would no longer be valid and the dynamic line widths would report the convolution between the spectral diffusion dynamics during the T_w period and the pulse duration.

[1] P. Schuster, G. Zundel, and C. Sandorfy, *The Hydrogen Bond Recent developments in theory and experiments* (North-Holland, Amsterdam, 1976).
[2] C. P. Lawrence and J. L. Skinner, J. Chem. Phys. **117**, 8847 (2002).
[3] C. P. Lawrence and J. L. Skinner, J. Chem. Phys. **118**, 264 (2003).
[4] R. Rey, K. B. Møller, and J. T. Hynes, J. Phys. Chem. A **106**, 11993 (2002).
[5] J. B. Asbury, T. Steinel, C. Stromberg, S. A. Corcelli, C. P. Lawrence, J. L. Skinner, and M. D. Fayer, J. Phys. Chem. A **108**, 1107 (2004).
[6] V. Daggett and A. Fersht, Nat. Rev. Mol. Cell Biol. **4**, 497 (2003).
[7] A. Almond and J. K. Sheehan, Glycobiology **10**, 329 (2000).
[8] D. Spangberg, R. Rey, J. T. Hynes, and K. Hermansson, J. Phys. Chem. B **107**, 4470 (2003).
[9] G. D. Smith, D. Bedrov, and O. Borodin, Phys. Rev. Lett. **85**, 5583 (2000).
[10] G. C. Pimentel and A. L. McClellan, *The Hydrogen Bond* (Freeman, San Francisco, 1960).
[11] U. Liddel and E. D. Becker, Spectrochim. Acta **10**, 70 (1957).
[12] W. Mikenda, J. Mol. Struct. **147**, 1 (1986).
[13] A. Novak, in *Structure and Bonding*, edited by J. D. Dunitz (Springer, Berlin, 1974), Vol. 18, p. 177.
[14] E. T. J. Nibbering and T. Elsaesser, Chem. Rev. (Washington, D.C.) **104**, 1887 (2004).
[15] J. Stenger, D. Madsen, P. Hamm, E. T. J. Nibbering, and T. Elsaesser, J. Phys. Chem. A **106**, 2341 (2002).
[16] J. Stenger, D. Madsen, P. Hamm, E. T. J. Nibbering, and T. Elsaesser, Phys. Rev. Lett. **87**, 027401 (2001).
[17] C. J. Fecko, J. D. Eaves, J. J. Loparo, A. Tokmakoff, and P. L. Geissler, Science **301**, 1698 (2003).
[18] S. Yeremenko, M. S. Pshenichnikov, and D. A. Wiersma, Chem. Phys. Lett. **369**, 107 (2003).
[19] T. Steinel, J. B. Asbury, S. A. Corcelli, C. P. Lawrence, J. L. Skinner, and M. D. Fayer, Chem. Phys. Lett. **386**, 295 (2004).
[20] H. Graener, G. Seifert, and A. Laubereau, Phys. Rev. Lett. **66**, 2092 (1991).
[21] S. Woutersen, U. Emmerichs, and H. J. Bakker, Science **278**, 658 (1997).
[22] R. Laenen, C. Rausch, and A. Laubereau, J. Phys. Chem. B **102**, 9304 (1998).
[23] R. Laenen, C. Rausch, and A. Laubereau, Phys. Rev. Lett. **80**, 2622 (1998).
[24] G. M. Gale, G. Gallot, F. Hache, N. Lascoux, S. Bratos, and J. C. Leicknam, Phys. Rev. Lett. **82**, 1068 (1999).
[25] H. J. Bakker, S. Woutersen, and H. K. Nienhuys, Chem. Phys. **258**, 233 (2000).
[26] S. Woutersen and H. J. Bakker, Phys. Rev. Lett. **83**, 2077 (1999).
[27] S. Bratos, G. M. Gale, G. Gallot, F. Hache, N. Lascoux, and J. C. Leicknam, Phys. Rev. E **61**, 5211 (2000).
[28] J. C. Deak, S. T. Rhea, L. K. Iwaki, and D. D. Dlott, J. Phys. Chem. A **104**, 4866 (2000).
[29] A. Pakoulev, Z. Wang, Y. Pang, and D. D. Dlott, Chem. Phys. Lett. **380**, 404 (2003).
[30] A. Pakoulev, Z. Wang, and D. D. Dlott, Chem. Phys. Lett. **371**, 594 (2003).
[31] T. Wang, D. Du, and F. Gai, Chem. Phys. Lett. **370**, 842 (2003).
[32] Z. Wang, Y. Pang, and D. D. Dlott, J. Chem. Phys. **120**, 8345 (2004).
[33] M. F. Kropman, H.-K. Nienhuys, S. Woutersen, and H. J. Bakker, J. Phys. Chem. A **105**, 4622 (2001).
[34] G. Gallot, N. Lascoux, G. M. Gale, J. C. Leicknam, S. Bratos, and S. Pommeret, Chem. Phys. Lett. **341**, 535 (2001).
[35] R. Laenen, K. Simeonidis, and A. Laubereau, J. Phys. Chem. B **106**, 408 (2002).
[36] D. Zimdars, A. Tokmakoff, S. Chen, S. R. Greenfield, M. D. Fayer, T. I. Smith, and H. A. Schwettman, Phys. Rev. Lett. **70**, 2718 (1993).
[37] A. Tokmakoff and M. D. Fayer, J. Chem. Phys. **103**, 2810 (1995).
[38] K. D. Rector and M. D. Fayer, Laser Chem. **19**, 19 (1999).
[39] P. Hamm, M. Lim, and R. M. Hochstrasser, Phys. Rev. Lett. **81**, 5326 (1998).
[40] J. B. Asbury, T. Steinel, and M. D. Fayer, J. Lumin. **107**, 271 (2004).
[41] S. Mukamel, Annu. Rev. Phys. Chem. **51**, 691 (2000).
[42] D. M. Jonas, Annu. Rev. Phys. Chem. **54**, 425 (2003).
[43] M. Khalil, N. Demirdoven, and A. Tokmakoff, J. Phys. Chem. A **107**, 5258 (2003).
[44] M. Khalil, N. Demirdoven, and A. Tokmakoff, Phys. Rev. Lett. **90**, 047401(4) (2003).
[45] J. B. Asbury, T. Steinel, C. Stromberg, K. J. Gaffney, I. R. Piletic, A. Goun, and M. D. Fayer, Chem. Phys. Lett. **374**, 362 (2003).
[46] J. D. Hybl, A. A. Ferro, and D. M. Jonas, J. Chem. Phys. **115**, 6606 (2001).
[47] R. R. Ernst, G. Bodenhausen, and A. Wokaun, *Nuclear Magnetic Resonance in One and Two Dimensions* (Oxford University Press, Oxford, 1987).
[48] J. B. Asbury, T. Steinel, C. Stromberg, K. J. Gaffney, I. R. Piletic, and M. D. Fayer, J. Chem. Phys. **119**, 12981 (2003).
[49] S. Corcelli, C. P. Lawrence, and J. L. Skinner, J. Chem. Phys. **120**, 8107 (2004).
[50] W. L. Jorgensen, J. Chandrasekhar, J. D. Madura, R. W. Impey, and M. L. Klein, J. Chem. Phys. **79**, 926 (1983).
[51] H. J. C. Berendsen, J. R. Grigera, and T. P. Straatsma, J. Phys. Chem. **91**, 6269 (1987).
[52] S. Mukamel, *Principles of Nonlinear Optical Spectroscopy* (Oxford University Press, New York, 1995).
[53] S. W. Rick, S. J. Stuart, and B. J. Berne, J. Chem. Phys. **101**, 6141 (1994).
[54] S. Corcelli, C. P. Lawrence, J. B. Asbury, T. Steinel, M. D. Fayer, and J. L. Skinner, J. Chem. Phys. **121**, 8897 (2004).
[55] T. Steinel, J. B. Asbury, and M. D. Fayer, J. Phys. Chem. B (in press).
[56] H.-K. Nienhuys, S. Woutersen, R. A. van Santen, and H. J. Bakker, J. Chem. Phys. **111**, 1494 (1999).
[57] D. Cringus, S. Yeremenko, M. S. Pshenichnikov, and D. A. Wiersma, J. Phys. Chem. B **108**, 10376 (2004).
[58] K. J. Gaffney, I. R. Piletic, and M. D. Fayer, J. Chem. Phys. **118**, 2270 (2003).
[59] T. Steinel, J. B. Asbury, and M. D. Fayer, presented at the 51th Annual Western Spectroscopy Association Conference, Asilomar, California, USA, 2004 (unpublished).
[60] T. Steinel, J. B. Asbury, and M. D. Fayer (unpublished).
[61] J. B. Asbury, T. Steinel, and M. D. Fayer, in *Femtosecond Laser Spectroscopy: Progress in Lasers*, edited by P. Hannaford (Kluwer, Brussels, 2004).
[62] W. M. Zhang, V. Chernyak, and S. Mukamel, J. Chem. Phys. **110**, 5011 (1999).
[63] S. Mukamel and R. F. Loring, J. Opt. Soc. Am. B **3**, 595 (1986).
[64] D. Kroh and A. Ron, Chem. Phys. Lett. **36**, 527 (1975).
[65] M. R. J. Healy, *Matrices for Statisticians* (Clarendon, Oxford, 1986).
[66] A. Tokmakoff, J. Phys. Chem. A **104**, 4247 (2000).
[67] J. D. Hybl, Y. Christophe, and D. M. Jonas, Chem. Phys. **266**, 295 (2001).

[68] J. B. Asbury, T. Steinel, C. Stromberg, K. J. Gaffney, I. R. Piletic, A. Goun, and M. D. Fayer, Phys. Rev. Lett. **91**, 237402 (2003).
[69] J. B. Asbury, T. Steinel, and M. D. Fayer, J. Phys. Chem. B **108**, 6544 (2004).
[70] W. de Boeij, M. S. Pshenichnikov, and D. A. Wiersma, Chem. Phys. Lett. **253**, 53 (1996).
[71] T. H. Joo, Y. W. Jia, J. Y. Yu, D. M. Jonas, and G. R. Fleming, J. Chem. Phys. **104**, 6089 (1996).
[72] K. F. Everitt, E. Geva, and J. L. Skinner, J. Chem. Phys. **114**, 1326 (2001).
[73] A. Piryatinski and J. L. Skinner, J. Phys. Chem. B **106**, 8055 (2002).
[74] C. P. Lawrence and J. L. Skinner, J. Chem. Phys. **117**, 5827 (2002).
[75] K. B. Møller, R. Rey, and J. T. Hynes, J. Phys. Chem. A **108**, 1275 (2004).
[76] C. P. Lawrence and J. L. Skinner, Chem. Phys. Lett. **369**, 472 (2003).
[77] M. Mezei and D. L. Beveridge, J. Chem. Phys. **74**, 622 (1981).
[78] H. Xu, H. A. Stern, and B. J. Berne, J. Phys. Chem. B **106**, 2054 (2002).